Dynamics of Q-switched laser annealing

D. H. Auston, J. A. Golovchenko, A. L. Simons, and C. M. Surko
Bell Laboratories, Murray Hill, New Jersey 07974

T. N. C. Venkatesan
Bell Laboratories, Crawford Hill Laboratory, Holmdel, New Jersey 07733

(Received 2 January 1979; accepted for publication 16 March 1979)

Using time-resolved optical-reflectivity measurements, the duration of the thin liquid layer accompanying Q-switched laser annealing in Si, Ge, and GaAs has been determined. The duration of this melted layer has been studied as a function of laser energy at 1.06- and 0.53-μm wavelength for both implanted and unimplanted samples. Thresholds for initiation of melting and damaging the surface are obtained directly. With the aid of channeling–Rutherford-backscattering measurements, the duration of melt necessary for annealing implanted samples is determined. Results for unimplanted silicon at 530 nm are compared with recent numerical calculations. In addition, measuremnts of the fall time of the reflectivity as the liquid-solid interface approaches the surface enables us to estimate regrowth velocities. A simple scheme is also discussed for efficient annealing with dual wavelengths.

PACS numbers: 42.60.Kg, 81.40.Ef

Laser annealing of ion-implanted semiconductors has received considerable interest in recent times, [1] and a basic understanding of the physical processes involved appears to be evolving. In two recent publications [2] preliminary results of a combination of time-resolved reflectivity and channeling measurements were used to experimentally show that typical annealing of silicon with a cw argon laser proceeds by solid-phase epitaxial regrowth while annealing with a Q-switched Nd-glass laser proceeds via liquid-phase epitaxial regrowth. In this letter we present new results for a wide variety of semiconductor materials, at different annealing laser wavelengths. We show that not only can the presence of a liquid layer be detected during the annealing process in all cases, but a careful study of the time structure and energy dependence yields comprehensive information on crystal-regrowth velocities and thresholds for annealing. These reflectivity results when correlated with RBS-channeling measurements provide a simple *in situ* criterion for determining the quality of annealing. Furthermore, the completeness of these experimntal results enables a useful comparison with recent theoretical calculations of the melting and recrystallization process.

The optical reflectivity of materials being laser annealed was monitored during the Q-switched laser irradiation by a small cw HeNe probe laser whose output, once reflected off the sample surface, was monitored in a fast (rise time ~ 3 ns) silicon avalanche photodiode. We have extended the previous measurement capability described in Ref. 2 by using a KDP frequency doubler so that annealing could be done with either a 1060- or 530-nm pulse. We have discovered that certain aspects of the annealing process are extremely sensitive to minute dust particles, etc., and that when suitable precautions are taken (i.e., degreasing with hot organic solvents, mechanical scrubbing, and a final HCl, H_2O_2, and H_2O rinse and spin dry) highly reproducible results are obtained.

Figure 1 shows a typical time-resolved reflectivity measurement for the case of 530-nm annealing of 30-kV, 10^{15}/cm^2 arsenic-implanted (100) silicon. (The incident pulse had a duration of 30 ns and energy of 2.75 J/cm^2.) As the annealing laser turns on, the initial reflectivity of the amorphous layer, R_a, rises with the increasing tempeature of the sample surface to a value R'_a when the surface melts, and an abrupt increase in reflectivity occurs due to the metallic nature of liquid silicon.[3] The reflectivity remains high at the value R_l as the liquid-solid interface penetrates more deeply into the sample and then reverses its direction some time after the annealing laser pulse has ended. As the liquid-solid interface proceeds towards the surface, the reflectivity decreases to R'_c of the hot solid. The surface is melted for a total time τ. The fall time τ_f is the time required for the regrowth front to move through one optical skin depth and is a measure of the regrowth velocity. As the crystal cools further, the room-temperature value R_c of the crystalline phase is obtained. One additional feature of Fig. 1 which is observed at moderately high annealing energies in silicon and germanium is a slight reduction in the refelctivity during the incident pulse. At temperatures well above the melting point,

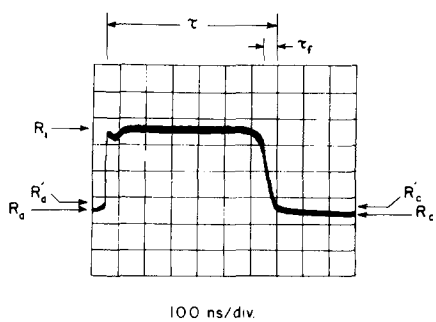

FIG. 1. Time-resolved reflectivity trace for 630-nm HeNe incident light polarized in the plane of incidence at 45° to the surface normal. Reflectivities of room-temperature amorphous silicon, amorphous silicon just prior to melting, metallic silicon, hot crystalline, and room-temperature silicon are characterized by R_a, R'_a, R_1, R'_c, and R_c respectively.

 0003-6951/79/110777-03$00.50

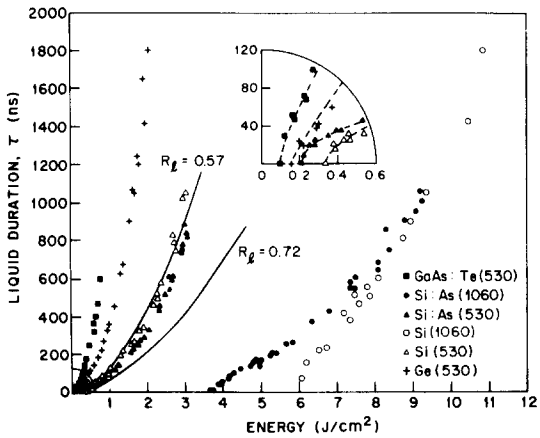

FIG. 2. Duration of the liquid layer for different materials and annealing wavelengths as a function of optical energy, as determined by time-resolved reflectivity. The particular doses of the implanted samples are mentioned in the text. The solid curves are numerical calculations of the melt dynamics for unimplanted silicon at 530 nm.

the optical constants of silicon and germanium change, and a reduced reflectivity might be expected.

Figure 2 contains a detailed plot of liquid duration times τ versus input laser energy density for Ge (unimplanted), GaAs (implanted with 50-keV Te at 10^{16}/cm^2), and silicon (unimplanted and implanted with 30-keV arsenic at 10^{15}/cm^2), the latter case for both 530- and 1060-nm anneals. For each case there is a well-defined threshold for melting. The frequency-doubled light is seen to be considerably more efficient in initiating the melt process in silicon than the 1060-nm output. Thus, the near agreement between implanted and unimplanted silicon results at 530 nm is not surprising in view of the large optical-absorption coefficients in both cases leading to efficient thermal conversion in the sample. Nevertheless, a clear difference exists in the thresholds for melting between the implanted and unimplanted case as seen in the magnified inset of Fig. 2. A clear understanding of the effect requires a detailed knowledge of both the thermal and optical properties of the amorphous silicon layer. Under the conditions of annealing neither of these are well known. In the unimplanted case at 1060 nm it is difficult to account for the initiation of melting without invoking nonlinear absorption process. Once the melt begins, however, its high absorption coefficient remedies this situation. For the case of implanted silicon at 1060 nm the increased absorption of the amorphous layer (500 Å thick in this case) is surely responsible for the reduced threshold. It is interesting to note that the ratio of the optical energies absorbed in the implanted silicon samples at 1060 and 530 nm is approximately 1 : 20, which compares favorably with the ratios of melt thresholds for these cases (taking an absorption constant of 10^4 cm^{-1} for the amorphous layer at 1060 nm). The energies required for melting Ge and GaAs at 530 nm are reduced from those of silicon due to the lower melting points. For each material and wavelength the highest energy point on the curves in Fig. 2 were taken just below the threshold for catastrophic surface damage.

Several calculations of the melt dynamics in silicon have been reported.[4-7] In Fig. 2 we have plotted calculations[7] of the melt duration in unimplanted silicon versus 530-nm pulse energy for two different values of the reflectivity in the liquid state, $R_l = 0.57$ and 0.72. The first case gives the best fit to the experiment, and is similar to the calculations of Baeri *et al.*[4] who used $R_l = 0.60$. The larger value of R_l, however, is closer to what one would expect for liquid silicon from published measurements of the optical constants.[3] Our He-Ne reflectivity measurements give $R_l \simeq 0.66$ at normal incidence if a Drude model is used to scale the wavelength from 633 to 530 nm. At high annealing energies R_l may be reduced to 0.63, as indicated by the dip in the reflectivity trace in Fig. 1.

It should be emphasized that the threshold for melting at the surface and the threshold for annealing implanted materials are not identical. The implanted silicon reported on in this work has an amorphous layer of silicon extending 468 ± 10 Å from the surface (as determined by electron microscopy). If the liquid layer formed during the annealing does not penetrate to this depth the final recrystallization will not proceed from undamaged material, and it may be anticipated that a polycrystalline surface layer will result upon cooling.[8] We therefore made RBS-channeling studies of implanted samples annealed with different laser energies so as to have different durations of liquid melts in order to determine the threshold for annealing in terms of τ. The channeling results obtained using 1.7-MeV α particles on (100) silicon are shown in Fig. 3. The surface peak in the aligned as-implanted sample corresponds to the previously described 468-Å amorphous layer. After a laser anneal with a 530-nm pulse, which results in a 40-ns liquid layer, only a slight improvement in the channeling is observed. However

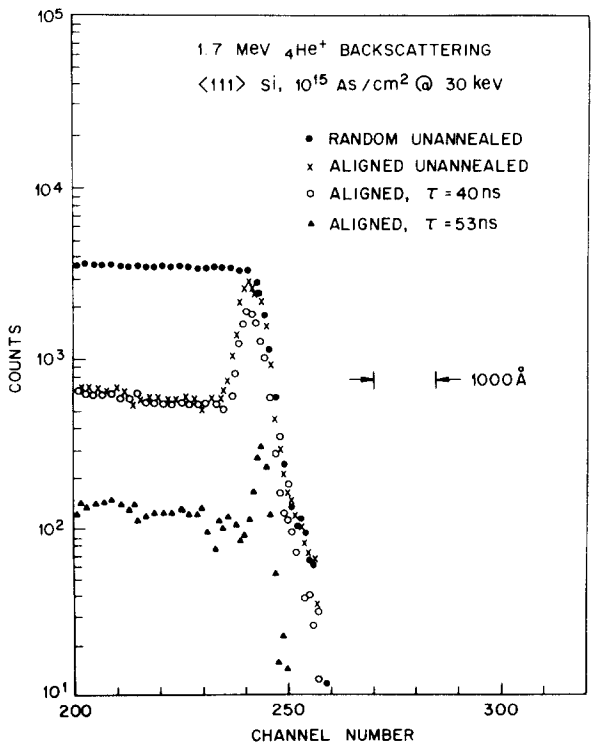

FIG. 3. Backscattering-channeling spectra of implanted silicon for two different melt durations illustrating threshold for complete recrystallization.

after an anneal giving a 53-ns liquid the sample completely recovers its crystallinity. We thus determine the liquid duration corresponding to a depth of 468 Å as ~ 45 ns.

The fall time τ_f of the reflectivity waveform is the time required for the solid-liquid interface to move through one optical skin depth as it approaches the surface. We can use it to estimate the regrowth velocity. For example, for the case in Fig. 1, when the melt lasts for a total time of 64 ns, the fall time was 50 ns, corresponding to a regrowth velocity of approximately 35 cm/s. For shorter melt durations, such as $\tau \simeq 45$ ns at the threshold for complete recrystalliztion, we find the regrowth velocity was approximately 240 cm/s. If we assume the melt front advances and receeds at approximately the same rate, a velocity of this magnitude would be adequate to completely melt the amorphous layer in 45 ns, consistent with the RBS spectra. Calculations[4,7] of the melt dynamics, however, suggest that the regrowth velocities should be larger by a factor of 2 or 3. The reason for this discrepancy is not clear.

Finally, we would like to comment on an interesting application of the data reported in Fig. 2. It is quite obvious that the 530-nm light is much more efficient in coupling to the solid than is the 1060-nm light. This might seem to be a mixed blessing in view of the fact that the process of frequency doubling to the shorter wavelength is done with at most $\sim 30\%$ efficiency. In our experiment this value was close to 10%. Nevertheless, all of the incident energy can be coupled to the solid with efficiencies, near the 530-nm case if the unconverted component of the incident beam is also allowed to irradiate the sample. This is because once the 530-nm light melts the top layer of silicon the absorption coefficient for the 1060-nm light increases dramatically, resulting in a high efficiency of coupling for this major component of the incident light. Only enough 530-nm light is necessary in applications to trigger the liquid layer. Thus, the full energy from large Nd laser systems is made available for annealing without complications such as doping level dependence[9] of the threshold or ultimate depth distributions known to exist for 1060-nm annealings.

In conclusion, we would like to stress that time-resolved reflectivity and channeling measurements may be used together to determine several physical quantities of interest in laser annealing. It should be clear that once a correlation between the results of these techniques is established, the former may alone be used as a convenient *in situ* means of controlling and evaluating the properties of laser-annealed materials for device applications.

Thanks are due to P. Petroff for providing guidance to our experiments via his electron microscope studies of laser annealed samples. J. Rodgers, R. D'Angelo, and E. Povilonis helped in sample preparation, and P. Smith with calculations. Also, useful conversations with D. Aspnes are acknowledged.

[1]Phys. Today **31**, 17–19 (1978), and references therein.
[2]D.H. Auston, C.M. Surko, T.N.C. Venkatesan, R.E. Slusher, and J.A. Golovchenko, Appl. Phys. Lett. **33**, 437 (1978); D.H. Auston, J.A. Golovchenko, P.R. Smith, C.M. Surko, and T.N.C. Venkatesan, Appl. Phys. Lett. **33**, 539 (1978). J.S. Williams, W.L. Brown, H.J. Leamy, J.M. Poate, J.W. Rodgers, D. Rousseau, G.A. Rozgonyi, J.A. Shelnutt, T.T. Sheng, *ibid.* p. 542.
[3]K.M. Shvarev, B.A. Baum, and P.V. Gel'd, Sov. Phys.–Semicond. **16**, 2111 (1975).
[4]P. Baeri, S.U. Campisano, G. Foti, and E. Rimini, Appl. Phys. Lett. **33**, 137 (1978).
[5]J.C. Wang, R.F. Wood, and P.P. Pronko, Appl. Phys. Lett. **33**, 455 (1978).
[6]I.B. Khaibullin, E.I. Shtyrkov, M.M. Zaripov, R.M. Bayzitov, and M.F. Galjautdinov, Radiat. Eff. **36**, 225 (1978).
[7]C.M. Surko, A.L. Simons, D.H. Auston, J.A. Golovchenko, and T.N.C. Venkatesan (unpublished).
[8]G. Foti, E. Rimini, G. Vitali, and M. Bertolotti, Appl. Phys. **14**, 189 (1977).
[9]T.N.C. Venkatesan, J.A. Golovchenko, J.M. Poate, P.L. Cowan, and G.K. Celler, Appl. Phys. Lett. **33**, 429 (1978).